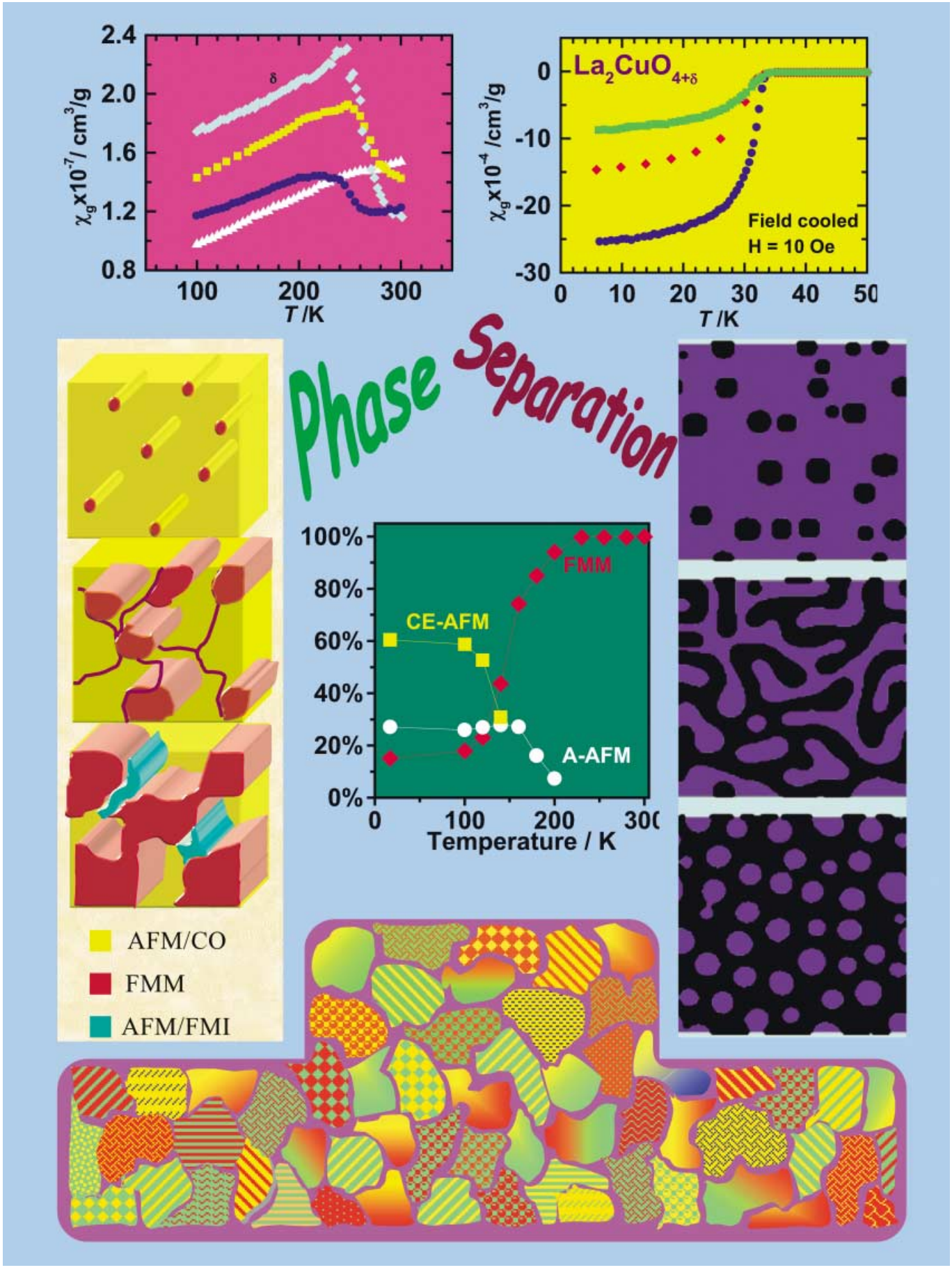

0947-6539/03/0904-0828 $ 20.00+.50/0 *Chem. Eur. J.* **2003**, *9*, No. 4

Phase Separation in Metal Oxides

C. N. R. Rao,*[a] P. V. Vanitha,[a] and Anthony K. Cheetham[b]

Abstract: A fascinating phenomenon, recently found to occur in certain transition-metal oxides, is phase separation wherein pure, nominally monophasic oxides of transition metals with well-defined compositions separate into two or more phases over a specific temperature range. Such phase separation is entirely reversible, and is generally the result of a competition between charge-localization and -delocalization, the two situations being associated with contrasting electronic and magnetic properties. Coexistence of more than one phase, therefore, gives rise to electronic inhomogeneity and a diverse variety of magnetic, transport, and other properties, not normally expected of the nominal monophasic composition. An interesting feature of phase separation is that it covers a wide range of length scales anywhere between 1–200 nm. While cuprates and manganates, especially the latter, provide excellent examples of phase separation, it is possible that many other transition-metal compounds with extended structures will be found to exhibit phase separation.

Keywords: magnetic properties · metal oxides · phase separation · rare earth manganates

Introduction

It is generally assumed that a single crystal of a compound is pure and monophasic, with an exact composition and a well-defined set of properties. While this is indeed true of most molecular and extended solids, it has been found in recent years that a few of the transition-metal oxides negate this presumption, and exhibit compositional and electronic inhomogeneities arising from the existence of more than one phase in crystals of nominally monophasic composition. The different phases in such materials have comparable compositions, and the phenomenon is commonly referred to as phase separation. One may be tempted to think that there is little new in this phenomenon. Afterall, there are many oxide systems in which there is intergrowth of related phases, as exemplified by the Aurivillius family of oxides of the general composition, $Bi_4A_{m+n-2}B_{m+n}O_{3(m+n)+6}$ (A = Ba or Bi, B = Ti, Nb etc).[1, 2] In the oxides of this family, it is common to find the presence of unit cells of the wrong $(m+n)$ values to intergrow along with the major phase (e.g., $(m+n)$ of 1 or 2 in a major phase corresponding to $(m+n)$ of 3). Similar intergrowths occur in cuprates of the type $Bi_2(CaSr)_{n+1}Cu_nO_{2n+4}$ and $Tl_2A_{n+1}Cu_nO_{2n+4}$ (A = Ca, Sr, Ba), as well as in the Ruddlesden–Popper series of oxides of the type $Sr_{n+1}Ti_nO_{3n+1}$.[1, 2] While the presence of intergrowths in the metal oxides such as the above affects the properties of the major phase, no new property or phenomenon seems to result from it. Our interest in this article is in phase-separated solids whose behavior is significantly different from what is expected of the nominal composition, and reflects a combination of disparate electronic, magnetic, and other properties associated with the different phases coexisting together. In certain cases, phase separation does indeed give rise to entirely new properties.

A good example of phase separation is that in $La_2CuO_{4+\delta}$, in which two phases with different oxygen stoichiometries coexist over a specific temperature range.[3] Thus, the cuprate with a nominal $\delta \approx 0.03$ separates into two phases below a certain temperature, one with a small oxygen excess ($\delta \sim 0.01$) and another with a higher oxygen excess ($\delta \sim 0.06$).[4] The two phases possess entirely different magnetic and electrical properties. Rare-earth manganates of the general composition, $Ln_{1-x}A_xMnO_3$ (Ln = rare earth, A = alkaline earth), display a variety of effects due to phase separation, giving rise to novel electronic and magnetic properties. The rare-earth manganates became popular because of the colossal magnetoresistance (CMR) exhibited by them.[5] CMR and related properties are generally explained on the basis of the double-exchange mechanism of electron hopping between the Mn^{3+} ($t_{2g}^3e_g^1$) and Mn^{4+} ($t_{2g}^3e_g^0$) ions. In this mechanism, the ferromagnetic alignment of the spins of the incomplete e_g orbitals of adjacent Mn ions is directly related to the rate of

[a] Prof. Dr. C. N. R. Rao, P. V. Vanitha
CSIR Centre of Excellence in Chemistry and
Chemistry and Physics of Materials Unit
Jawaharlal Nehru Center for Advanced Scientific Research
Jakkur P.O., Bangalore, 560 064 (India)
Fax: (+91) 80-846-270
E-mail: cnrrao@jncasr.ac.in

[b] Prof. Dr. A. K. Cheetham
Materials Research Laboratory
University of California
Santa Barbara, CA-93106 (USA)

  0947-6539/03/0904-0829 $ 20.00+.50/0

hopping of the electrons, giving rise to an insulator–metal transition at the ferromagnetic Curie temperature (T_C). In the ferromagnetic state ($T < T_C$), the material is metallic, but is an insulator in the paramagnetic state ($T > T_C$). Jahn–Teller distortion associated with the Mn^{3+} ions and charge-ordering of the Mn^{3+} and Mn^{4+} ions compete with double exchange and promote the insulating behavior and antiferromagnetism.[5] Charge-ordering in these materials is also closely linked to the ordering of the e_g orbitals. The nature of phase separation in the manganates depends on the average size of the A-site cations, carrier concentration or the composition (value of x), temperature, and other external factors such as magnetic and electric fields. Phases with different charge densities (carrier concentrations) as well as magnetic and transport properties coexist as carrier-rich ferromagnetic (FM) clusters or domains along with a carrier-poor antiferromagnetic (AFM) phase. Such an electronic phase separation giving rise to microscopic or mesoscopic inhomogeneous distribution of electrons results in rich phase diagrams that involve various types of magnetic structures.[6] What is noteworthy is that electronic phase separation is likely to be a general property of solids with correlated electrons such as the large family of transition-metal oxides. There are indications that many of the unusual magnetic and transport properties of oxide materials arise from phase separation.[3, 6]

The term phase separation or segregation implies the presence of at least two distinct phases in the sample, but the relative fractions may vary anywhere from a dilute regime, involving small domains of the minor phase (or clusters) in the matrix of the major phase, to a situation in which the fractions of the two phases is comparable. Thus, FM clusters present randomly in an AFM host matrix often give rise to a glassy behavior. As the FM clusters in an AFM matrix grow in size to become reasonably sized domains, due to effect of temperature, composition, or an applied magnetic field, the system acquires the characteristics of a genuine phase-separated system. We shall discuss the various scenarios in phase-separated rare-earth manganates in this article by presenting some of the recent results in the form of phase diagrams and schematic illustrations of the spatial distribution of the coexisting phases. We shall also briefly examine the features of phase separation in oxygen excess La_2CuO_4. Before discussing the results on these oxide systems, we shall examine the general features of phase separation in solids.[3, 6]

Phase Separation: The Phenomenon

Thermodynamic, equilibrium phase separation is distinct from phase separation caused by inhomogeneties in chemical composition, such as those due to non-uniformity in impurity distribution, as it can have an electronic origin or could also arise from the presence of magnetic impurities. Such phase separation can be controlled or changed by temperature, magnetic fields, and other external factors. In both these types of phase separation, a high carrier density favors ferromagnetic ordering and/or metallicity. If the carrier concentration is not sufficient, ferromagnetic ordering can occur in one portion of the crystal, the rest of the crystal remaining insulating and antiferromagnetic. In electronic phase separation, the concentration of the charge carriers giving rise to ferromagnetism and/or metallicity in a part of the crystal causes mutual charging of the two phases. This gives rise to strong Coulomb fields, which may mix the conducting ferromagnetic and insulating antiferromagnetic phases in order to lower the Coulomb energy. When the carrier concentration is small, the conducting ferromagnetic regions are separated forming droplets as in Figure 1a. At higher carrier concentrations, the volume of the ferromagnetic phase

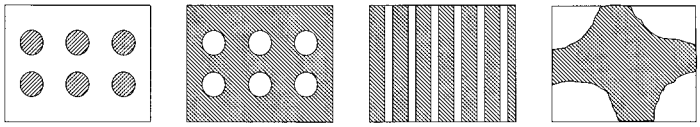

Figure 1. Microscopic phase-separated state giving rise to a) an insulating state with ferromagnetic (conducting/metallic) droplets, b) a conducting state where a ferromagnetic (conducting) part of the crystal has separated (insulating) droplets, and c) charge-stripes. A macroscopic phase separation state is shown in d). Hatched portions represent the ferromagnetic regions with high carrier concentration (and are therefore conducting)

increases rendering the droplets to coalesce, giving rise to a situation shown in Figure 1b. Electronic phase separation has been observed in magnetic semiconductors such as heavily doped EuSe and EuTe. Here, the main portion of the crystal is antiferromagnetic at low temperatures and the conducting electrons occur in the ferromagnetic droplets. A magnetic-field-induced insulator to metal transition, giving rise to high magnetoresistance, is accompanied by an increase in the size of the ferromagnetic droplets.

Impurity phase separation is different from electronic phase separation in that there is no mutual charging of the phases in the former. Here also, magnetic fields increase the size of the magnetic domains or regions. Impurity atom diffusion has to be sufficiently large to give rise to phase separation in such systems. The case of oxygen-excess La_2CuO_4 is one such example.

The case of rare-earth manganates, $Ln_{1-x}A_xMnO_3$ (Ln = rare earth, A = alkaline earth), is one in which the ferromagnetic phase is conducting and the antiferromagnetic phase is insulating. Depending on x or the carrier concentration, we can have a situation such as that shown in Figure 1a or b. The phase separation scenario here is somewhat complex because the transition from the metallic to the insulating state is not sharp, and the domains of the two phases are often sufficiently large to give rise to well-defined signatures in neutron scattering or diffraction experiments. However, one may consider the large magnetoresistance in these systems to be a consequence of the electronic phase separation. In the presence of Coulomb interaction, the microscopically charged inhomogeneous state is stabilized, giving rise to clusters of one phase embedded in another. The size of the clusters depends on the competition between double exchange and Coulomb forces. Electronic phase separation with phases of different charge densities is generally expected to give rise to nanometer scale clusters. This is because large phase-sepa-

0947-6539/03/0904-0830 $ 20.00+.50/0 *Chem. Eur. J.* **2003**, *9*, No. 4

rated domains would break up into small pieces because of Coulomb interactions. The shapes of these pieces could be droplets or stripes (Figure 1a–c).

One can visualize phase separation arising from disorder as well. The disorder can arise from the size mismatch of the A-site cations in the perovskite structure.[7] Such phase separation is seen in the $(La_{1-y}Pr_y)_{1-x}Ca_xMnO_3$ (LPCM) system in terms of a metal–insulator transition induced by disorder. The size of the clusters depends on the magnitude of disorder. The smaller the disorder, the larger would be the size of the clusters. This could be the reason why high magnetoresistance occurs in systems with small disorder.

Microscopically homogeneous clusters are usually of the size of 1–2 nm in diameter dispersed in an insulating or charge-localized matrix as seen in Figure 1a. Such a phase-separation scenario bridges the gap between the double-exchange model and the lattice distortion models. A number of recent papers on manganates show that in addition to microscopic phase separation there can also be mesoscopic phase separation whereby the length scale is between 30–200 nm, arising from the comparable energies of the ferromagnetic metallic and antiferromagnetic insulating states. In certain manganate compositions, mesoscopic as well as microscopic phase separation has been observed. In LPCM and other manganates, the occurrence of multiple phases has also been noticed.

The techniques required to identify phase separation in different length scales vary. For example, diffraction techniques can be used to examine macroscopic phase separation (Figure 1d), for which distinct features occur in the diffraction patterns due to the different phases in the system. Techniques such as NMR spectroscopy, on the other hand, give information on the local environment at a microscopic level. It is often difficult to identify electronic phase separation based on magnetic measurements because of the sensitivity of phase separation to magnetic fields. Thus, magnetic fields transform the antiferromagnetic insulating state to the ferromagnetic metallic state. However, transport measurements, under favorable conditions, can provide valuable information on phase separation.

Lanthanum Cuprate

La_2CuO_4 is an insulating layered oxide thst contains CuO_2 sheets.[2] It is antiferromagnetic, but the AFM order is destroyed on doping it with holes. Hole doping is accomplished by introducing excess oxygen between the LaO layers or by substituting La partly by a divalent cation such as Sr^{2+}. A neutron diffraction study[4] of $La_2CuO_{4.03}$ synthesized under high oxygen pressure showed that it undergoes a reversible macroscopic phase separation below a certain temperature, T_{ps}, into two nearly identical orthorhombic phases with δ values of ~ 0.01 and ~ 0.08. Phase separation in this oxygen-excess cuprate is evidenced from resistivity, magnetic susceptibility, specific heat, NMR, and NQR measurements, which show anomalies around T_{ps}.[8] In Figure 2, we show the phase diagram of $La_2CuO_{4+\delta}$ (upto $\delta = 0.07$) constructed by Chou and Johnston.[8] The $\delta = 0.01$ and 0.08 phases possess entirely

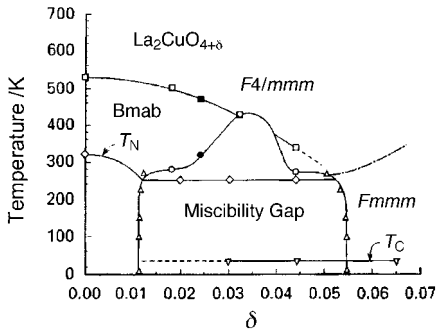

Figure 2. Phase diagram of $La_2CuO_{4+\delta}$ (reproduced with permission from ref. [8]).

different properties, the former being an AFM insulator ($T_N = 250$ K) and the latter a superconductor ($T_C \approx 35$ K). Accordingly, magnetic susceptibility measurements on a sample of $La_2CuO_{4+\delta}$ show both the AFM and superconducting transitions[8] as shown in Figure 3. The transitions exhibit

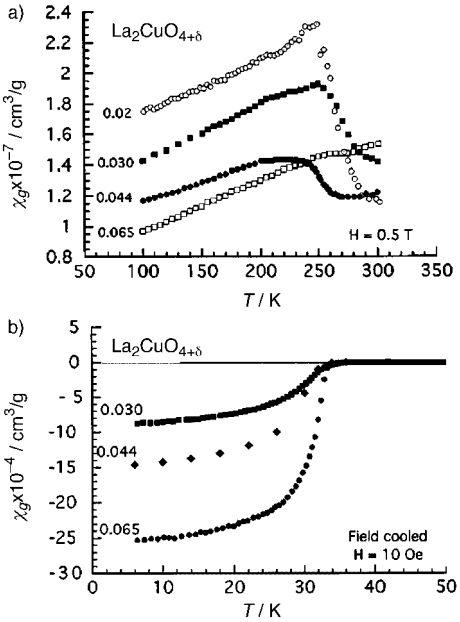

Figure 3. Temperature dependence of magnetic susceptibility of $La_2CuO_{4+\delta}$ showing antiferromagnetic and superconducting transitions (reproduced with permission from ref. [8]).

considerable thermal hysteresis. TEM images reveal the domain structure of the oxygen-rich and -poor phases with a minimum dimension of 30–150 nm.[9] Phase separation in $La_2CuO_{4+\delta}$ can be visualized from the spatial distribution of the AFM and superconducting regions presented in Figure 4.[10]

Inhomogeneous doping of the CuO_2 planes gives rise to hole-rich (metallic) one-dimensional features (charge stripes) due to the concentration of holes in periodic walls superposed on AFM stripes (Figure 1c). The stripes are a consequence of phase separation, arising from preferred hole dopings with independent dispersions. The stripes are charge-driven rather than spin-driven.[11, 12] Such stripes due to the presence of hole-rich and hole-poor regions are also seen in nickelates of

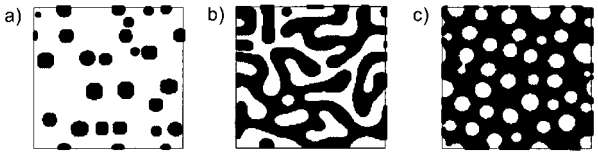

Figure 4. Schematic representation of the growth of the antiferromagnetic (white) and superconducting (black) phases with increasing doping or δ value (reproduced with permission from ref. [10]).

the type $La_2NiO_{4+\delta}$.[11] Phase separation and stripes are found in $La_{2-x}Sr_xCuO_4$ ($0.0 < x < 0.15$) as well.[13, 14] In adiition, this system shows another kind of phase separation. When the hole concentration is greater than 0.085, the cuprate exhibits two superconducting transitions at 15 K and 30 K.[14] When it is less than 0.02, AFM order coexists with a spin-glass phase at low temperatures.[15]

Rare-Earth Manganates

A wide range of compositions of the rare-earth manganates, $Ln_{1-x}A_xMnO_3$ (Ln = rare earth, A = alkaline earth), exhibit charge-ordering.[5] Charge- and AFM-ordering may occur at the same temperature or at different temperatures. The Mn^{3+} (d_{z^2}) orbitals and the associated lattice distortions develop long-range order, and such orbital-ordering occurs with charge ordering in many of the manganates, but it is always accompanied by AFM ordering. In $Ln_{1-x}A_xMnO_3$, small Ln and A ions stabilize the charge-ordered state. Thus, $Pr_{0.7}Ca_{0.3}MnO_3$, with an average A-site cation radius, $\langle r_A \rangle$, of 1.18 Å, charge-orders around 230 K (T_{CO}) in the paramagnetic state, becoming antiferromagnetic at 170 K; it is an insulator and does not show ferromagnetism in the absence of a strong magnetic field. $La_{0.7}Ca_{0.3}MnO_3$ ($\langle r_A \rangle = 1.27$ Å), on the other hand, is an FM metal below the T_C ($T_C \approx 250$ K) and a paramagnetic insulator above the T_C. $La_{0.5}Sr_{0.5}MnO_3$ ($\langle r_A \rangle =$ 1.26 Å) is metallic both in the FM and paramagnetic states, whereas $Nd_{0.5}Sr_{0.5}MnO_3$ ($\langle r_A \rangle = 1.24$ Å) shows a transition from a FM metallic state to an AFM charge-ordered state around 150 K. The charge-ordered states in these manganates are associated with CE-type AFM-ordering, whereby the Mn^{3+} and Mn^{4+} ions are arranged as in a checker board. The CE-type AFM charge-ordered state in $Ln_{1-x}A_xMnO_3$ is associated with the ordering of $3x^2 - r^2$ or $3y^2 - r^2$ type orbitals at the Mn^{3+} site. The Jahn – Teller distortion that accompanies orbital ordering stabilizes the CE-type AFM state relative to the FMM state. Orbital and spin ordering occur without charge ordering in the manganates that show A-type antiferromagnetism.

Evidence for charge ordering in the rare-earth manganates is found in the crystal structures at low temperatures. A charge-ordering transition is marked by a resistivity anomaly, specially if the transition is first order.[5] Magnetization shows an abrupt change or a peak depending on the nature of the transition. Accordingly, the transition in $Nd_{0.5}Sr_{0.5}MnO_3$ at 150 K from the FM state to the AFM charge-ordered state ($T_{CO} = T_N$) is accompanied by a sharp increase in resistivity and a decrease in the magnetization (Figure 5). In $Pr_{0.6}Ca_{0.4}$-

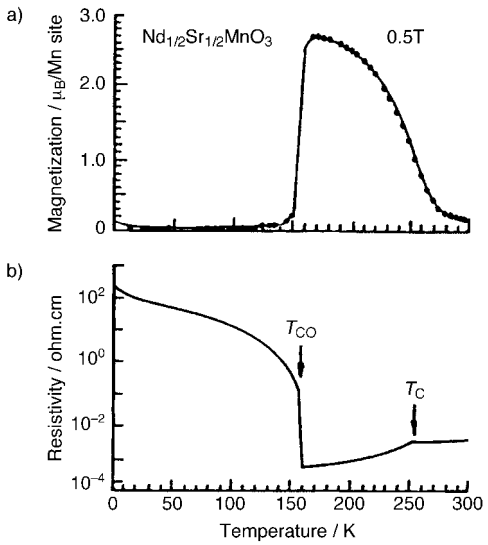

Figure 5. Temperature variation of a) magnetization and b) resistivity of $Nd_{0.5}Sr_{0.5}MnO_3$ (reproduced with permission from ref. [5b]).

MnO_3 ($\langle r_A \rangle = 1.18$ Å) the paramagnetic ground state is charge-ordered and becomes antiferromagnetic on cooling (Figure 6). This manganate shows a small peak in magnetization at T_{CO}. Furthermore, well below T_N the magnetic susceptibility shows clear indications for the presence of

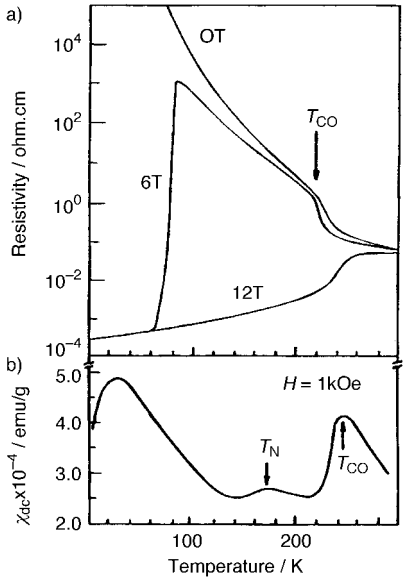

Figure 6. Temperature variation of a) resistivity and b) magnetic susceptibility of $Pr_{0.6}Ca_{0.4}MnO_3$ (reproduced with permission from ref. [5b]).

ferromagnetic interactions (see Figure 6). The charge-ordered states in the manganates can be transformed to a FM metallic state by the application of magnetic fields, the strength of the field depending on the robustness of the charge-ordered state. The charge-ordered state in the manganates with small A-site cations is often unaffected by strong magnetic fields or by doping the Mn site by cations such as Ru^{4+} and Cr^{3+}. These dopants transform the charge-ordered state in both $Nd_{0.5}Sr_{0.5}MnO_3$ and $Pr_{0.6}Ca_{0.4}MnO_3$ into a FM metallic state.

0947-6539/03/0904-0832 $ 20.00+.50/0 *Chem. Eur. J.* **2003**, *9*, No. 4

In Figure 7, we show the phase diagrams of $La_{1-x}Ca_xMnO_3$ and $Pr_{1-x}Ca_xMnO_3$. In the former, charge ordering occurs in the $x \approx 0.5-0.8$ range, while in the latter charge ordering

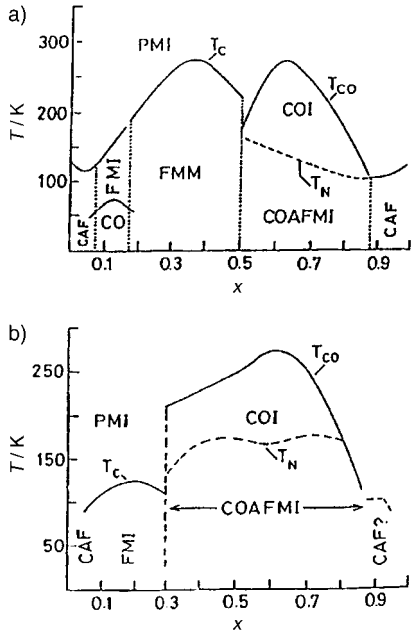

Figure 7. Phase diagrams of a) $La_{1-x}Ca_xMnO_3$ and b) $Pr_{1-x}Ca_xMnO_3$. CAF, canted antiferromagnet; CO, charge-ordered state; FMI, ferromagnetic insulator; FMM, ferromagnetic metal; PMI, paramagnetic insulator; COI, charge-ordered insulator (paramagnetic); COAFMI, charge-ordered antiferromagnetic insulator (reproduced with permission from ref. [16]).

occurs over the $x \approx 0.3-0.8$ range. These differences are essentially due to the effect of the size of the A-site cations, the smaller size favoring the charge-ordered insulating state. From Figure 7, we see that the charge-ordered regime is prominent at large values of x. Thus, the $x > 0.5$ compositions in $Ln_{1-x}Ca_xMnO_3$ are almost entirely in the charge-ordered regime when Ln = La or Pr. This regime is referred to as the electron-doped regime and the $x < 0.5$ compositions as the hole-doped regime. There is marked electron-hole asymmetry in these manganates, ferromagnetism and metallicity not being encountered in the electron-doped regime.[16]

At low dopant levels (low x values, say $x < 0.1$), FM clusters are found to be present in an antiferromagnetic host matrix in $Ln_{1-x}Ca_xMnO_3$, often giving rise to a spin-glass behavior. A similar situation obtains when $x > 0.9$. The coexistence of charge-ordered (AFM) and FM domains, the sizes of which are affected by the composition (x value), relative sizes of A-site cations, temperature, magnetic field, and cation doping, arises from electronic phase separation,[6, 17, 18] giving rise to anomalous magnetic and transport properties. In $La_{1-x-y}Pr_yCa_xMnO_3$ ($x = 0.37$), mesoscopic phase separation into submicrometer-scale charge-ordered regions (3–20 nm) and FM metallic domains have been observed in electron microscopic images.[19] In $Nd_{0.5}Sr_{0.5}MnO_3$, phase segregation of the FM metallic and CE-AFM charge-ordered phases along with a A-type AFM phase has been observed.[20] The point to note is that phase separation in all these materials is a consequence of the competition between charge localization and charge-delocalization, the two being associated with contrasting magnetic and transport properties.[6, 17]

As mentioned earlier, coexistence of the FM metallic and the AFM insulator phases due to electronic phase separation (inhomogeneous distribution of charge densities) cannot be a long-range phenomenon owing to the high coulomb energy cost. Therefore, we observe a microscopically inhomogeneous state with FM clusters of 1–2 nm in diameter dispersed in an insulating (charge-localized) matrix as in Figure 1a. Evidence for such microscopic phase separation in the manganates is found from various physical measurements[6, 17, 21] (e.g., spin-glass behavior or canted-spin ordering as seen at low temperatures in $Pr_{0.6}Ca_{0.4}MnO_3$, see Figure 6). The cause of mesoscopic phase separation found in some manganate compositions lies in the comparable energies of the FM metallic and insulating phases, and the large strain mismatch of the domains of the two phases.[22]

Some Recent Results

We shall now briefly examine some of the recent findings on rare earth manganates. Based on neutron scattering and diffraction studies, Radaelli et al.[23, 24] have shown tunable mesoscopic phase separation in $Pr_{0.7}Ca_{0.3}MnO_3$. Intragranular strain-driven mesoscopic phase segregation (5–20 nm) between two insulating phases (one charge-ordered and another spin-glass) occurs below T_{CO}. The charge-ordered phase orders antiferromagnetically and the other remains a spin-glass. On the application of a magnetic field, most of the material goes to a FM state. Microscopic phase separation (0.5–2 nm) is present at all temperatures, especially in the spin-glass phase at low temperatures. These results are shown in the form of a phase diagram in Figure 8.

As mentioned earlier, submicrometer-sized phase separation involving FM and charge-ordered AFM domains has been found in $La_{5/8-y}Pr_yCa_{3/8}MnO_3$. By varying y, the volume fraction and the domain size of the FM and charge-ordered phases can be varied.[19] In Figure 9, a schematic diagram to describe the coexistence of the two phases is shown. Electrical conduction in this manganate occurs through a percolative mechanism because of phase separation. The phase diagram of $(La_{1-y}Pr_y)_{0.7}Ca_{0.3}MnO_3$ showing the dependence of phase separation on the composition and temperature[25] is shown in Figure 10. Clearly, phase separation is sensitive to the cation size and size disorder.

$La_{0.5}Ca_{0.5}MnO_3$ changes to a FM phase on cooling to 220 K (T_C) and then to a charge-ordered AFM phase around 150 K (T_{CO}). This manganate is best described as magnetically phase separated over a wide range of temperatures.[26, 27] At low temperatures ($T < T_{CO}$), FM metallic domains are trapped in the charge-ordered AFM matrix, giving rise to percolative metallic conduction. The fraction of the FM phase at low temperatures is highly dependent on the thermal treatment. Even within the FM phase, in the $T_{CO} < T < T_C$ region, there is phase separation. A second crystallographic phase, probably without magnetic order, has been identified.[27] The phase diagram of $La_{1-x}Ca_xMnO_3$ in the $0.47 \le x \le 0.5$ range (Figure 11) reveals the nature of phase separation. Magnetization

  0947-6539/03/0904-0833 $ 20.00+.50/0

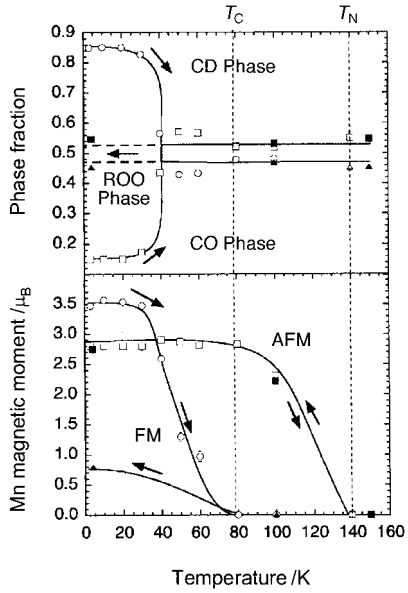

Figure 8. Fractions and magnetism of the coexisting phases $Pr_{0.7}Ca_{0.3}MnO_3$ from multiphase Rietveld refinements of neutron data. Top: Phase fractions of charge-ordered (AFM) phase (squares), ferromagnetic charge-delocalized (CD), and reverse orbital-ordered (ROO) weakly ferromagnetic spin-glass phase (triangles) on zero-field cooling (filled symbols) and warming after 7 T field processing at 3 K (open symbols). Arrows indicate the direction of cooling/heating. Bottom: magnetic moments per manganese atom for the individual phases (symbols as in top panel) (reproduced with permission from ref. [24]).

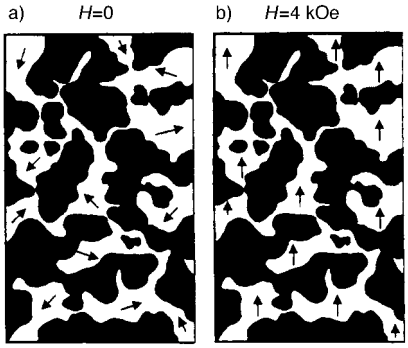

Figure 9. Schematic diagram showing the coexistence of the charge-ordered insulating (dark area) and FM metallic (white area) domains in $La_{1-x-y}Pr_yCa_xMnO_3$. Arrows show alignment in a magnetic field (reproduced with permission from ref. [19]).

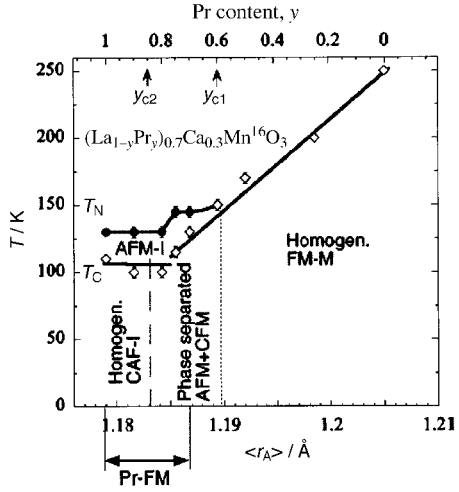

Figure 10. Phase diagram of the $(La_{1-y}Pr_y)_{0.7}Ca_{0.3}MnO_3$. The diamonds and circles show the T_C and T_N values. The bottom x axis shows the average A cation radius $\langle r_A \rangle$. The low-temperature state is homogeneous for $y > 0.8$ (canted AFM insulator, CAF-I) and for $y < 0.6$ (FM metal). In the range $0.6 \leq x \leq 0.8$ the magnetic state is an inhomogeneous mixture of slightly canted ferromagnetic (CFM) and AFM regions. The T_N and T_C transition temperatures coincide for $x = 0.6$. A ferromagnetic contribution of Pr moments is found in the interval of the Pr concentration marked as Pr-FM (reproduced with permission from ref. [25]).

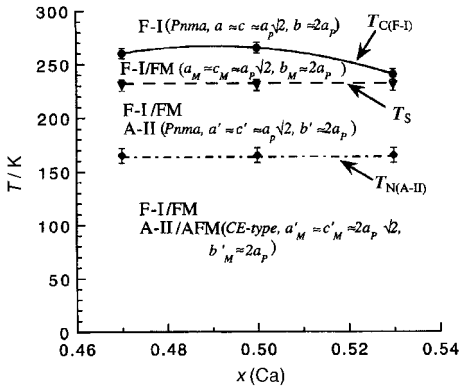

Figure 11. Phase diagram of $La_{1-x}Ca_xMnO_3$ in the range of compositions $0.47 \leq x \leq 0.53$. The horizontal curves separate, going from top to bottom: i) the FM transition of the F-I crystallographic phase at $\sim$260 K; ii) the formation of the low-temperature A-II phase, which appears at $\sim$230 K; and iii) the AFM transition that occurs in the A-II structure at $\sim$160 K (T_N). As shown in the diagram, the ferromagnetically ordered F-I phase and the antiferromagnetically ordered A-II phase coexist at low temperatures (reproduced with permission from ref. [27]).

studies show three phase separated regimes: $T_C > T > T_O$, $T_O > T > T_{CO}$ and $T < T_{CO}$, in which T_O is the onset temperature below which the cooling field plays an unbalancing role in favor of the FM state.[26] It is in the last regime that minority FM domains are embedded in the AFM matrix. In the first regime near the T_C, the FM phase grows freely with the application of a magnetic field.

The occurrence of a phase-separated state below T_{CO} (T_N) in some of the manganate compositions was pointed out earlier. In Figure 12, we illustrate the phenomenon schematically in the case of $Nd_{0.55}(Sr_{0.17}Ca_{0.83})_{0.45}MnO_3$.[28] The situation is even more complex in $Nd_{0.5}Sr_{0.5}MnO_3$. High resolution X-ray and neutron diffraction investigations show that $Nd_{0.5}Sr_{0.5}MnO_3$ separates into three macroscopic phases at low temperatures.[20] The phases involved are the high-temperature FMM phase, the orbitally ordered A-type AFM phase, and the charge-ordered CE-type AFM phase. On cooling this manganate, the A-type AFM phase starts manifesting itself around 220 K, with the charge-ordered AFM phase appearing at 150 K (as expected from Figure 5). At the so-called FM metallic-charge-ordered AFM transition, all the three phases coexist, and this situation continues down to very low temperatures as shown in Figure 13. In Figure 14, we show the percentage volume fraction of the different phases in the presence and absence of a magnetic field.[29] Phase segregation in this system seems to depend crucially on the Mn^{4+}/Mn^{3+} ratio, a ratio slightly greater than unity stabilizes the A-type AFM phase. Thus, $Nd_{0.45}Sr_{0.55}MnO_3$ has the A-type AFM structure.

0947-6539/03/0904-0834 $ 20.00+.50/0 *Chem. Eur. J.* **2003**, *9*, No. 4

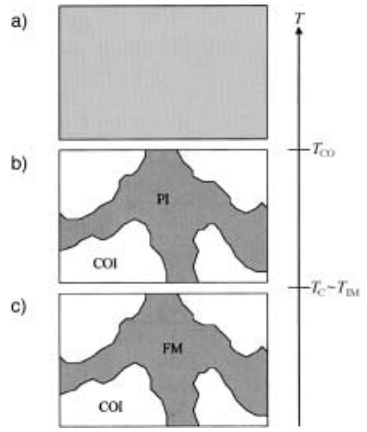

Figure 12. Schematic illustrations for the temperature variation of phase separated state in $Nd_{0.55}(Sr_{0.17}Ca_{0.83})_{0.45}MnO_3$: a) $T > T_{CO}$, b) $T_C < T < T_{CO}$, c) $T < T_C$. COI, PI, and FM, stand for the charge-ordered insulating, paramagnetic insulating, and ferromagnetic metallic phases, respectively (reproduced with permission from ref. [28]).

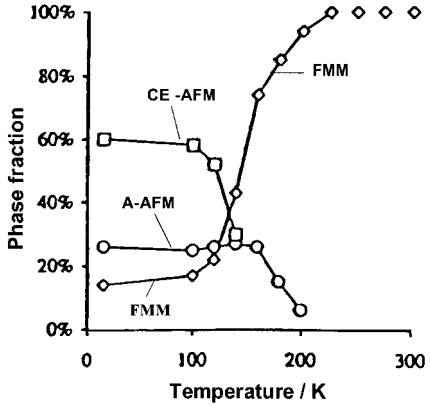

Figure 13. Variation in the percentage of the different phases of $Nd_{0.5}Sr_{0.5}MnO_3$ with temperature (reproduced with permission from ref. [20]).

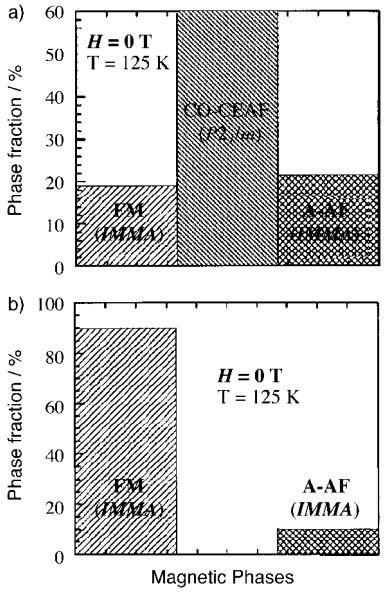

Figure 14. Schematic diagram of the percentage volume fractions of different phases of $Nd_{0.5}Sr_{0.5}MnO_3$ under a) $H = 0$ T and b) 6 T (reproduced with permission from ref. [29]).

The few case studies of the rare-earth manganates described above should suffice to illustrate how phase separation is of common occurrence in this family of oxides. Phase separation occurs in layered manganates,[30] electron-doped manganates,[31] $Ln_{1-x}A_xMnO_3$ $(x > 0.5)$, and in $Ca_{1-x}Bi_xMnO_3$.[32]

Conclusion

Phase separation in metal oxide systems has emerged to become a phenomenon of importance, because of the diversity of properties found in the rare earth manganates. In Figure 1, we showed a few possible scenarios of phase separation schematically. These scenarios roughly represent the experimental observations in the rare-earth manganates. Phase separation has been observed recently in real space with atomic-scale resolution.[33] It seems likely that phase separation will be found in materials in which the electronic or magnetic properties vary strikingly over extremely narrow composition ranges. For most classes of materials this is not the case, but in highly correlated systems, instability towards phase separation and formation of inhomogeneous states may be an intrinsic property.[34] For example, phase separation is suspected to be responsible for the occurrence of two magnetic transitions in $Sr_3CuIrO_{6+\delta}$.[35] The compositional FM–AFM transition accompanying changes in electron bandwidth found in $La_{1-x}Y_xTiO_3$, coexistence of FM and paramagnetic phases in $La_{1-x}Sr_xCoO_3$, and the compositional AFM–FM transition in $Ca_{2-x}La_xRuO_4$ are all likely to be associated with phase separation.[6] What is important to note is that phase separation occurs over a large length scale from a few angstroms to a few hundred nanometers. The domain sizes of the component phases clearly determine the properties of the material.

Acknowledgement

This work was supported by BRNS (DAE, India) and the MRSEC program of the National Science Foundation under Award No. DMROO-80034.

[1] C. N. R. Rao, J. M. Thomas, *Acc. Chem. Res.* **1985**, *18*, 113.
[2] a) C. N. R. Rao, B. Raveau, *Transition Metal Oxides*, 2nd ed., Wiley-VCH, Weinehim, **1999**; b) C. N. R. Rao, J. Gopalakrishnan, *New Directions in Soild State Chemistry*, 2nd ed., Cambridge University Press, **1997**.
[3] a) *Phase Separation in Cuprate Superconductors* (Eds.: K. A. Müller, G. Benedek), World Scientific, Singapore, **1993**; b) *Phase Separation in Cuprate Superconductors* (Eds.: E. Sigmund, K. A. Müller), Springer, Heidelberg, **1994**; c) *Stripes and Related Phenomena* (Eds.: A. Bianconi, N. L. Saini), Kluwer Academic, Dordrecht, **2000**.
[4] a J. D. Jorgensen, B. Dabroski, S. Pei, D. G. Hinks, L. Soderholm, B. Morosin, J. E. Schirber, E. L. Venturini, D. S. Ginley, *Phys. Rev. B* **1988**, *38*, 11337; b) B. Dabrowski, J. D. Jorgensen, D. G. Hinks, S. Pei, D. R. Richards, H. B. Vanfleet, D. L. Decker, *Physica C* **1989**, *162–164*, 99.
[5] a) *Colossal Magnetoresistance, Charge-Ordering and Related Properties of Manganese Oxides* (Eds.: C. N. R. Rao, B. Raveau), World Scientific, Singapore, **1999**; b) C. N. R. Rao, A. Arulraj, A. K. Cheetham, B. Raveau, *J. Phys.: Condens. Matter* **2000**, *12*, R83; c) Y.

Tokura, *Colossal Magnetoresistive Oxides*, Gordon and Breach, New York, **2000**; d) A. P. Ramirez, *J. Phys.: Condens. Matter* **1997**, *9*, 8171; e) C. N. R. Rao, A. K. Cheetham, R. Mahesh, *Chem. Mater.* **1996**, *8*, 2421; f) C. N. R. Rao, *Chem. Eur. J.* **1996**, *2*, 1499.

[6] a) E. Dagotto, T. Hotta, A. Moreo, *Phys. Rep.* **2001**, *344*, 1; b) A. Moreo, S. Yunoki, E. Dagotto, *Science* **1999**, *283*, 2034; c) E. L. Nagaev, *Phys.-Usp.* **1996**, *39*, 781.

[7] a) L. M. Rodriguez-Martinez, J. P. Attfield, *Phys. Rev. B* **1996**, *54*, R15622; b) J. P. Attfield, *Chem. Mater.* **1998**, *10*, 3239.

[8] F. C. Chou, D. C. Johnston, *Phys. Rev. B* **1996**, *54*, 572, and references therein.

[9] J. Ryder, P. A. Midgley, R. Exley, R. J. Beynon, D. L. Yalis, L. Afalfiz, J. A. Wilson, *Physica C* **1991**, *173*, 9.

[10] J. Wang, D. Y. Xing, J. Dong, P. H. Hor, *Phys. Rev. B* **2000**, *62*, 9827.

[11] O. Zachar, S. A. Kivelson, V. J. Emery, *Phys. Rev. B* **1998**, *57*, 1422.

[12] a) C. N. A. van Duin, J. Zaanen, *Phys. Rev. Lett.* **1998**, *80*, 1513; b) R. S. Markiewicz, *Phys. Rev B* **2000**, *62*, 1252, and references therein; c) V. V. Moshchalkov, J. Vancken, L. Trappeniers, *Phys. Rev. B* **2001**, *64*, 214504 and references therein.

[13] N. A. Nemov, V. R. Belosludov, *Phys. C* **1998**, *308*, 55.

[14] B. Lorenz, Z. G. Li., T. Honma, P.-H. Hor, *Phys. Rev. B* **2002**, *65*, 144522.

[15] M. Matsuda, M. Fujita, K. Yamada, R. J. Birgeneau, Y. Endoh, G. Shirane, *Phys. Rev. B* **2002**, *65*, 134515.

[16] K. V. Sarathy, P. V. Vanitha, R. Seshadri, A. K. Cheetham, C. N. R. Rao, *Chem. Mater.* **2001**, *13*, 787.

[17] C. N. R. Rao, P. V. Vanitha, *Curr. Opin. Solid State Mater. Sci.* **2002**, *6*, 97.

[18] B. Raveau, M. Hervieu, A. Maignan, C. Martin, *J. Mater. Chem.* **2001**, *11*, 29.

[19] M. Uehara, S. Mori, C. H. Chen, S.-W. Cheong, *Nature* **1999**, *399*, 560.

[20] P. M. Woodward, D. E. Cox, T. Vogt, C. N. R. Rao, A. K. Cheetham, *Chem. Mater.* **1999**, *11*, 3528.

[21] J. M. de Teresa, M. R. Ibarra, P. A. Algarabel, C. Ritter, C. Marquina, J. Blasco, J. Garcia, A. del Moral, Z. Arnold, *Nature* **1997**, *386*, 256.

[22] P. B. Littlewood, *Nature* **1999**, *399*, 529.

[23] D. E. Cox, P. G. Radaelli, M. Marezio, S.-W. Cheong, *Phys. Rev. B* **1998**, *57*, 3305.

[24] P. G. Radaelli, R. M. Ibberson, D. N. Argyriou, H. Casalta, K. H. Andersen, S.-W. Cheong, J. F. Mitchell, *Phys. Rev. B* **2001**, *63*, 172419.

[25] A. M. Balagurov, V. Yu. Pomjakushin, D. V. Sheptyakov, V. L. Aksenov, P. Fischer, L. Keller, O. Yu. Gorbenko, A. R. Kaul, N. A. Babushkina, *Phys. Rev. B* **2001**, *64*, 024420.

[26] a) R. S. Freitas, L. Ghivelder, P. Levy, F. Parisi, *Phys. Rev. B* **2002**, *65*, 104403 and references therein; b) F. Parisi, P. Levy, L. Givelder, G. Polla, D. Vega, *Phys. Rev. B* **2001**, *63*, 144419.

[27] Q. Huang, J. W. Lynn, R. W. Erwin, A. Santoro, D. C. Dender, V. N. Smolyaninova, K. Ghosh, R. L. Greene, *Phys. Rev. B* **2000**, *61*, 8895.

[28] A. Machida, Y. Moritomo, E. Nishibori, M. Takata, M. Sakata, K. Ohoyama, S. Mori, N. Yamamoto, A. Nakamura, *Phys. Rev. B* **2000**, *62*, 3883.

[29] C. Ritter, R. Mahendiran, M. R. Ibarra, L. Morellon, A. Maignan, B. Raveau, C. N. R. Rao, *Phys. Rev. B* **2000**, *61*, R9229.

[30] S. H. Chun, Y. Lyanda-Geller, M. B. Salamon, R. Suryanarayanan, G. Dhalene, A. Revcolevschi, *J. Appl. Phys.* **2001**, *90*, 6307.

[31] a) M. Respaud, J. M. Broto, H. Rakoto, J. Vanacken, P. Wagner, C. Martin, A. Maignan, B. Raveau, *Phys. Rev. B* **2001**, *63*, 144426; b) P. A. Algarabel, J. M. de Teresa, B. Garcia-Landa, L. Morellon, M. R. Ibarra, C. Ritter, R. Mahendiran, A. Maignan, M. Hervieu, C. Martin, B. Raveau, A. Kurbakov, V. Tournov, *Phys. Rev. B* **2002**, *65*, 104437.

[32] P. N. Santhosh, J. Goldberger, P. M. Woodward, T. Vogt, W. P. Lee, A. J. Epstein, *Phys. Rev. B* **2000**, *62*, 14928.

[33] Ch. Renner, G. Aeppli, B.-G. Kim, Y-A. Soh, S.-W. Cheong, *Nature* **2002**, *416*, 518.

[34] D. Khomskii, *Physica B* **2000**, *280*, 325.

[35] A. Niazi, P. L. Paulose and E. V. Sampathkumaran, *Phys. Rev. Lett.* **2002**, *88*, 107202.

  0947-6539/03/0904-0836 $ 20.00+.50/0